

# Scaling Laws and Mesoscopic Modeling of Thermal Conductivity in Carbon Nanotube Materials

Alexey N. Volkov and Leonid V. Zhigilei\*

University of Virginia, Department of Materials Science and Engineering,  
395 McCormick Road, Charlottesville, Virginia 22904-4745, USA

(Received 12 March 2010; published 28 May 2010)

The scaling laws describing the thermal conductivity in random networks of straight conducting nanofibers are derived analytically and verified in numerical simulations. The applicability of the scaling laws to more complex structures of interconnected networks of bundles in carbon nanotube (CNT) films and mats is investigated in mesoscopic simulations. The heat transfer in CNT materials is found to be strongly enhanced by self-organization of CNTs into continuous networks of bundles. The thermal conductivity of CNT films varies by orders of magnitude depending on the length of the nanotubes and their structural arrangement in the material.

DOI: 10.1103/PhysRevLett.104.215902

PACS numbers: 65.80.-g, 44.05.+e, 61.46.-w

An exceptionally high thermal conductivity of carbon nanotubes (CNTs) makes them one of the most promising structural elements in the design of new nanomaterials for heat management applications. Indeed, the values of room temperature thermal conductivity along the individual CNTs predicted in theoretical [1,2] and experimental [3,4] studies range from several hundreds of  $\text{W m}^{-1} \text{K}^{-1}$  to  $\sim 6600 \text{ W m}^{-1} \text{K}^{-1}$  and by far exceed the values characteristic of most conventional materials. Measurements of the thermal conductivity  $k$  of “bulk” CNT-based materials, such as CNT mats, films, and vertically aligned CNT arrays [5–9], however, reveal values that range from  $\sim 0.1 \text{ W m}^{-1} \text{K}^{-1}$  to  $\sim 200 \text{ W m}^{-1} \text{K}^{-1}$ , which are much smaller than one would anticipate from the conductivity of individual CNTs. The results of recent molecular dynamics simulations [10–13] and an experimental study [14] indicate that thermal coupling between adjacent CNTs is weak and the value of  $k$  is limited by the intertube heat transfer rather than the heat conduction within individual CNTs. These considerations, combined with experimental and theoretical analysis of  $k$  performed for three-dimensional (3D) networks of CNTs, have led to a suggestion that a compact random network of CNTs has properties typical of thermally insulating materials [9]. In this Letter we use a combination of theoretical analysis of scaling laws for  $k$  in generic nanofibrous materials and mesoscopic simulations of heat transfer in CNT films with realistic network structures to show that, depending on the length and spatial arrangement of nanotubes, the CNT materials can be either excellent heat conductors or thermal insulators. The high structural sensitivity of  $k$ , revealed in the simulations, points to the feasibility of the targeted design of CNT-based materials for controlling and directing the heat flow at nano- and microscale.

In order to obtain the thermal conductivity scaling laws relevant to CNT films with preferential orientation of nanotubes within the planes of the films [8], we start from the analysis of a two-dimensional (2D) isotropic network of

randomly dispersed straight nanotubes. Calculation of the thermal conductivity is based on a model of random thermal contacts between soft-core spherocylinders (SCs) [15] of length  $L_T$  and external radius  $R_T$  that can freely intersect each other. The analysis is performed under the assumption that  $k$  is defined by the intertube thermal contact resistance and every nanotube  $i$  in the sample is characterized by a single value of temperature  $T_i$ . The heat flux at a contact between SCs  $i$  and  $j$  is  $Q_{ij} = \sigma_c(T_j - T_i)$ , where the intertube contact conductance,  $\sigma_c$ , is assumed to be the same for all contacts,  $\sigma_c = \sigma_c 0$ .

An example of 2D systems used in the calculations is shown in Fig. 1(a). The temperatures of all SCs crossing the left and right boundaries are maintained at fixed temperatures. The temperatures of all “internal” SCs are calculated from the balance of incoming and outgoing

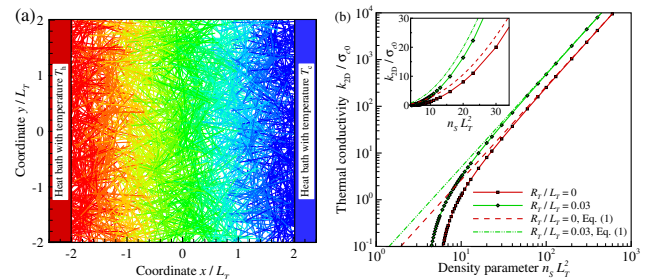


FIG. 1 (color online). An example of a 2D system used in calculations of thermal conductivity,  $k_{2D}$ , within a model of random contacts between soft-core SCs (a) and the results of the calculations performed for different values of  $\bar{n}_S = n_S L_T^2$  and two values of  $\bar{R}_T = R_T / L_T$  (b). In (a), the system consists of 1848 SCs,  $\bar{n}_S = 100$ ,  $\bar{R}_T = 0$ , and the SCs are colored by their temperature. In (b), the red and green symbols and solid curves correspond to the values obtained in the numerical calculations for  $\bar{R}_T$  equal to 0 and 0.03, respectively; the corresponding dashed and dash-dotted lines are the predictions of the analytical scaling law given by Eq. (1). The inset in (b) shows an enlarged view of a part of the plot in a regular scale.

heat fluxes in each SC. The thermal conductivity,  $k_{2D}$ , is then determined from the Fourier law adopted for the 2D case. The calculations, performed for several values of aspect ratio of SCs  $\bar{R}_T = R_T/L_T$  and a broad range of dimensionless density parameter  $\bar{n}_S = n_S L_T^2$  ( $n_S$  is the surface number density of SCs), predict a quadratic scaling of the 2D thermal conductivity with the density parameter,  $k_{2D} \propto \bar{n}_S^2$ , for “dense” SC networks at  $\bar{n}_S > 20$  [Fig. 1(b)]. The conductivity drops faster than  $\bar{n}_S^2$  for dilute networks, when  $\bar{n}_S$  approaches the percolation threshold [16].

In order to explain the scaling law,  $k_{2D} \propto \bar{n}_S^2$ , evident from the numerical calculations for dense networks, we perform a theoretical analysis of  $k_{2D}$ . The analytical solution for a dense 2D network composed of SCs with arbitrary  $\bar{R}_T$  can be written as [17]

$$k_{2D} = \sigma_{c0} \frac{\bar{n}_S^2}{12\pi} [1 + 8\pi\bar{R}_T + (72 + 6\pi^2)\bar{R}_T^2 + 96\pi\bar{R}_T^3 + 24\pi^2\bar{R}_T^4]. \quad (1)$$

The quadratic dependence on  $\bar{n}_S$  predicted by Eq. (1) matches the asymptotic behavior of the results of numerical calculations at  $\bar{n}_S \rightarrow \infty$  [Fig. 1(b)]. Moreover, Eq. (1) provides a good quantitative description of the numerical results at high  $\bar{n}_S$  (the difference is less than 1% for  $\bar{n}_S \geq 100$ ). With a decrease in the density parameter, the numerical results deviate from Eq. (1) due to the gradual decomposition of the network into quasiclusters poorly connected with each other.

A similar theoretical evaluation can be performed for 3D systems of randomly distributed and oriented SCs. The conductivity of a dense 3D system of SCs with arbitrary  $\bar{R}_T$  can be written as [17]

$$k_{3D} = \frac{\sigma_{c0}}{R_T} \frac{\pi\bar{n}_V^2}{36} (1 + 16\bar{R}_T + 80\bar{R}_T^2 + 192\bar{R}_T^3 + 153.6\bar{R}_T^4), \quad (2)$$

where  $\bar{n}_V = n_V L_T^3 R_T$  is the dimensionless density parameter and  $n_V$  is the volume number density of SCs. The results of numerical simulations performed for 3D systems with  $\bar{R}_T \geq 0.003$  confirm the validity of Eq. (2) for sufficiently large  $\bar{n}_V$ , with the difference between the numerical and analytical predictions being less than 1% for  $\bar{n}_V \geq 60$ .

Since for high-aspect-ratio SCs the material mass density,  $\rho$ , is proportional to  $n_S L_T$  and  $n_V L_T^3$  in the 2D and 3D cases, respectively, the dependences given by Eqs. (1) and (2) suggest the quadratic scaling with both  $\rho$  and  $L_T$ ,  $k_{2D}, k_{3D} \propto \rho^2 L_T^2$ . These scaling laws are in agreement with the results of Monte Carlo simulations of the electrical conductivity  $\sigma_{3D}$  of 3D percolating networks dominated by contact resistance [18], where the quadratic scaling law,  $\sigma_{3D} \propto \rho^2$ , was observed. The scaling law  $k_{3D} \propto \rho^2 L_T^2$  is also consistent with the results of a theoretical analysis performed for 3D systems of high-aspect-ratio cylindrical fibers [19]. The scaling law  $k_{3D} \propto \rho^2 L_T^2$ , however, contra-

dicts the results of more recent studies where a different dependence of  $k_{3D} \propto \rho L_T$  is derived analytically [12] and used for interpretation of experimental data [9]. Although the full details of the derivation are not provided in Ref. [12], the 3D model of random contacts between rod-like particles is similar to the one used in the derivation of Eq. (2). Therefore, we believe that the scaling law  $k_{3D} \propto \rho L_T$  was obtained in Ref. [12] erroneously.

In order to adopt Eq. (1) for calculation of thermal conductivity of anisotropic CNT materials characterized by the preferential in-plane orientation of CNTs, we consider a film composed of independent 2D layers stacked on top of each other and separated by a distance of  $\Delta z$ . The in-plane conductivity of the film,  $k_{xx}^{\text{film}} = k_{2D}/\Delta z$ , can be found from Eq. (1) and, for a film composed of high-aspect-ratio single-walled CNTs, can be written as

$$k_{xx}^{\text{film}} = \frac{\sigma_{c0}}{12\pi} \left( \frac{\rho L_T}{\rho_T} \right)^2 \Delta z, \quad (3)$$

where  $\rho_T = 2\pi R_T n_\sigma m_C$  is the linear mass density of a nanotube of a given radius  $R_T$ ,  $n_\sigma$  is the number density of carbon atoms on the surface of a CNT, and  $m_C$  is the mass of a carbon atom. The out-of-plane conductivity of the film,  $k_{zz}^{\text{film}}$ , can be found assuming that all nanotubes in a layer have the same temperature [17]:

$$k_{zz}^{\text{film}} = \frac{2\sigma_{c0}}{\pi} \left( \frac{\rho \Delta z}{\rho_T} \right)^2 \Delta z. \quad (4)$$

Equations (3) and (4) suggest that the thermal conductivity of dense films composed of 2D layers of SCs is highly anisotropic. For a film of (10,10) CNTs ( $R_T = 6.785 \text{ \AA}$ ) with  $L_T = 200 \text{ nm}$ , the ratio of the thermal conductivities,  $k_{zz}^{\text{film}}/k_{xx}^{\text{film}} = 24(\Delta z/L_T)^2$ , can be estimated to be  $1.7 \times 10^{-3}$  by assuming  $\Delta z = 2R_T + \delta h_0$ , where  $\delta h_0 = 3.144 \text{ \AA}$  is the equilibrium distance between surfaces of parallel CNTs [20].

While the idealized systems of randomly arranged straight SCs, discussed above, allow for analytical evaluation of the dependence of the thermal conductivity on the material density and the parameters of the nanofibers, the applicability of the scaling laws given by Eqs. (1)–(4) to real nanofibrous materials requires further verification. In particular, the structure of CNT films can be described as a continuous network of intertwined CNT bundles with a substantial bending of individual CNTs. To investigate the heat transfer in CNT films and mats, we perform a series of mesoscopic simulations that explicitly account for the complex structure of these materials.

The network structures of interconnected CNT bundles are generated in simulations performed with a mesoscopic dynamic model [20,21] that represents each individual CNT as a sequence of stretchable cylindrical segments. The dynamic behavior of CNTs is governed by a mesoscopic force field that accounts for the internal stretching, bending, and buckling of nanotubes, as well as for the

van der Waals interactions among the CNTs. The initial systems used in the simulations consist of straight (10,10) CNTs randomly distributed within layers stacked to form films with thicknesses of up to 200 nm and density of  $0.2 \text{ g cm}^{-3}$ , typical for CNT films and buckypaper [8]. In the course of dynamic mesoscopic simulations the systems of CNTs are observed to undergo fast (within nanoseconds) self-assembly into continuous networks of bundles [20] similar to the ones observed in experimental images of CNT films and mats [8]. The network structures, e. g., Figure 2, largely retain the initial anisotropy, with nanotube bundles preferentially oriented in the plane of the film.

The calculations of the thermal conductivity of the networks of CNT bundles are performed with an approach similar to the one described above for the systems composed of straight SCs. In order to account for the broad range of possible geometrical arrangements of the interacting CNTs in the network structures, a model based on a special “heat transfer” function  $\psi(r)$  is developed. In this model,

$$\sigma_c = \sigma_{c0} \frac{\Psi}{\Psi_0}, \quad \Psi = n_\sigma^2 \int_{S_1} \int_{S_2} \psi(r) dS_1 dS_2, \quad (5)$$

where  $r$  is the distance between points on the surfaces of the CNT segments and the integration is performed over the surfaces of the CNT segments. The use of the heat transfer function ensures a continuous transition between the limiting cases of parallel and perpendicular CNTs explored in atomistic simulations [9–13] and recent experi-

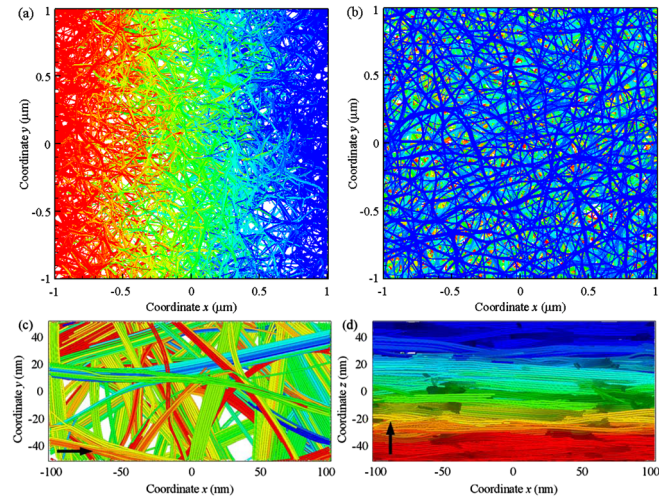


FIG. 2 (color online). The structure of a continuous network of CNT bundles generated in a mesoscopic dynamic simulation and used in the calculations of the thermal conductivities,  $k_{xx}^{\text{network}}$  and  $k_{zz}^{\text{network}}$ . The heat flux is in the direction of the  $x$  axis in (a, c) and in the direction of the  $z$  axis in (b, d) as indicated by the black arrows in (c) and (d). The nanotubes are colored by their temperature. The sample consists of 24 681 (10,10) CNTs with length of  $1 \mu\text{m}$  each. Only a layer with 50 nm thickness is shown in the top view of the film in (a).

ments [14]. Based on the results reported for parallel (10,10) CNTs [10], we set  $\psi(r) = 1$  at  $r \leq 8 \text{ \AA}$ , and use a cubic function that drops to zero at the cutoff distance of the carbon-carbon interatomic potential ( $10.2 \text{ \AA}$  [20]) at larger  $r$ . The constant  $\sigma_{c0}$  can be chosen to match the value of  $\sigma_c$  predicted in atomistic simulations for a geometrical configuration of CNTs with  $\Psi = \Psi_0$ . In this work we use the value of  $\sigma_{c0} = 5 \times 10^{-11} \text{ W K}^{-1}$  predicted in atomistic Green’s function calculations for two (10,10) CNTs crossing each other at a  $90^\circ$  angle [9].

The values of the thermal conductivity within the plane of preferred orientation of CNTs and perpendicular to the plane,  $k_{xx}^{\text{network}}$  and  $k_{zz}^{\text{network}}$ , are calculated by connecting the corresponding boundary planes to two heat baths maintained at different temperatures and evaluating the heat fluxes and temperature gradients established in the samples (Fig. 2). The values of  $k_{xx}^{\text{network}}$  are much higher than  $k_{xx}^{\text{film}}$  and  $k_{3D}$  (Fig. 3). This difference can be attributed to the bundle structure of the CNT network, with bundles providing “tight” arrangements of CNTs with larger contact area as compared to the random arrangements of CNTs assumed in the derivations of Eqs. (1)–(4).

The calculations predict a large difference (by more than 2 orders of magnitude) between  $k_{xx}^{\text{network}}$  and  $k_{zz}^{\text{network}}$ . The dependences on  $L_T$  are also very different, with a strong scaling of the in-plane conductivity,  $k_{xx}^{\text{network}} \propto L_T^{2.2}$ , and a much weaker scaling of the out-of-plane conductivity,  $k_{zz}^{\text{network}} \propto L_T^{0.59}$ . The weak scaling of  $k_{zz}^{\text{network}}$ , rather than complete independence of  $L_T$  expected for systems with perfect in-plane orientation of CNTs, e.g., Eq. (4), can be attributed to the out-of-plane inclination of CNT bundles in the network structures [Fig. 2(d)]. The observation of the strong anisotropy of the thermal conductivity in the networks of CNT bundles is consistent with experimental measurements of the thermal transport in anisotropic CNT-based materials [5–7]. The high structural sensitivity of the thermal conductivity, with 9 to 24 times difference between the values predicted for a random arrangement of straight CNTs and an interconnected network of bundles (Fig. 3), along with the strong dependence of  $k_{xx}^{\text{network}}$  on  $L_T$ , provide a hint for explaining the large variability of experimental data reported in the literature [5–8], with room temperature values measured for CNT mats and films ranging from  $15$  to  $220 \text{ W m}^{-1} \text{ K}^{-1}$ . This range is consistent with the calculated values of  $k_{xx}^{\text{network}}$  that span the range from  $0.8$  to  $205 \text{ W m}^{-1} \text{ K}^{-1}$  for a moderate material density of  $0.2 \text{ g cm}^{-3}$  and nanotube length from  $100 \text{ nm}$  to  $1 \mu\text{m}$ .

The ultralow ( $0.13$ – $0.2 \text{ W m}^{-1} \text{ K}^{-1}$ ) values of  $k$  recently reported for 3D isotropic CNT networks with densities comparable to the one used in our calculations and CNT length of  $5$ – $15 \mu\text{m}$  [9], however, are by far out of range of the computational predictions. The scaling down of the thermal conductance,  $\sigma_{c0}$ , by an order of magnitude, suggested in Ref. [9] as a way to account for the increase in the

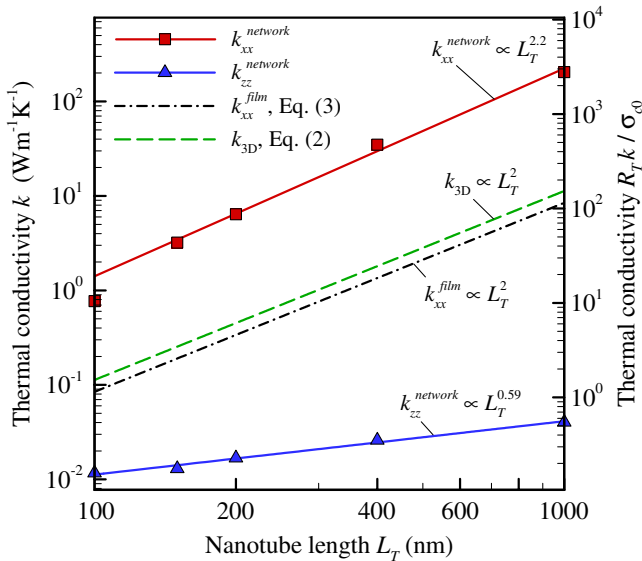


FIG. 3 (color online). Thermal conductivity  $k$  as a function of nanotube length  $L_T$  for systems composed of (10,10) CNTs with material density of  $0.2 \text{ g cm}^{-3}$ . Symbols show the results of the calculations performed for continuous networks of CNT bundles obtained in mesoscopic simulations. The red squares and blue triangles correspond to the calculations of in-plane and out-of-plane conductivities of the anisotropic networks. The solid lines are the root-mean-square power fits to the data points, with the point for  $L_T = 100 \text{ nm}$  excluded from the fit for  $k_{xx}^{\text{network}}$ . The green dashed and black dash-dotted lines show the predictions of the analytical scaling laws given by Eqs. (2) and (3), respectively. The value of out-of-plane conductivity  $k_{zz}^{\text{film}} = 5.7 \times 10^{-4} \text{ W m}^{-1} \text{ K}^{-1}$  predicted by Eq. (4) is out of the range shown in the plot. Dimensional values of  $k$  are calculated with  $\sigma_{c0} = 5 \times 10^{-11} \text{ W K}^{-1}$ . Values of  $k_{xx}^{\text{film}}$  and  $k_{zz}^{\text{film}}$  are calculated with  $\Delta z = 2R_T + \delta h_0 = 16.714 \text{ \AA}$ .

effective resistance of intertube contacts under conditions of high contact density, helps to reconcile the experimental data with the erroneous (see discussion above) linear scaling law  $k_{3D} \propto \rho L_T$ . To match the values of  $0.2 \text{ W m}^{-1} \text{ K}^{-1}$  at  $L_T = 5 \text{ }\mu\text{m}$  with Eqs. (2) or (3), however, the scaling of  $\sigma_{c0}$  by more than 3 orders of magnitude (and even more for the network of bundles obtained in the mesoscopic simulations) would be required, making it harder to justify. A detailed structural analysis of the CNT samples used in Ref. [9] would be needed to explain the lower, compared to earlier reports [5–8], values of thermal conductivity.

In summary, the theoretical analysis of nanofibrous materials with thermal transport properties governed by inter-fiber contact resistance suggests a strong quadratic dependence on the length of the nanofibers for the thermal conductivity of isotropic 3D systems of randomly dispersed straight nanofibers and in-plane conductivity of quasi-2D films composed of disordered layers of nanofibers. A similar superquadratic dependence is revealed

for random networks of CNT bundles produced in mesoscopic dynamic simulations. The values of the thermal conductivity in the networks of bundles significantly, by almost an order of magnitude, exceed the values predicted for the random arrangements of individual nanotubes. This increase is explained by an efficient heat transfer along the bundles, with each bundle serving as a “highway” for the thermal transport in the continuous network of bundles. The strong structural dependence of the thermal transport properties of the CNT networks explains the large variability of the experimental data reported for CNT films and mats and suggests that a detailed structural characterization of the materials is required for an adequate interpretation of the experimental measurements.

Financial support of this work is provided by NASA (Grant No. NNX07AC41A) and AFOSR (Grant No. FA9550-09-1-0245). Computational support is provided by NCCS at ORNL (Project No. MAT009).

\*lz2n@virginia.edu

- [1] S. Berber, Y.-K. Kwon, and D. Tománek, *Phys. Rev. Lett.* **84**, 4613 (2000).
- [2] S. Maruyama, *Physica (Amsterdam)* **323B**, 193 (2002).
- [3] P. Kim *et al.*, *Phys. Rev. Lett.* **87**, 215502 (2001).
- [4] E. Pop *et al.*, *Nano Lett.* **6**, 96 (2006).
- [5] J. Hone *et al.*, *Appl. Phys. Lett.* **77**, 666 (2000).
- [6] P. Gonnet *et al.*, *Curr. Appl. Phys.* **6**, 119 (2006).
- [7] I. Ivanov *et al.*, *Appl. Phys. Lett.* **89**, 223 110 (2006).
- [8] M. E. Itkis *et al.*, *Nano Lett.* **7**, 900 (2007).
- [9] R. S. Prasher *et al.*, *Phys. Rev. Lett.* **102**, 105901 (2009).
- [10] H. Zhong and J. R. Lukes, *Phys. Rev. B* **74**, 125403 (2006).
- [11] S. Maruyama *et al.*, *J. Thermal Sci. Tech.* **1**, 138 (2006).
- [12] Y. Chalopin, S. Volz, and N. Mingo, *J. Appl. Phys.* **105**, 084301 (2009).
- [13] Z. Xu and M. J. Buehler, *ACS Nano* **3**, 2767 (2009).
- [14] J. Yang *et al.*, *Appl. Phys. Lett.* **96**, 023 109 (2010).
- [15] I. Balberg *et al.*, *Phys. Rev. B* **30**, 3933 (1984).
- [16] The percolation threshold  $\bar{n}_{SP}$  determined in calculations performed for slender rods ( $R_T = 0$ ) and systems with the size of  $128L_T$  is found to be equal to 5.64, which is in a good agreement with previously reported values of 5.71 [G. E. Pike and C. H. Seager, *Phys. Rev. B* **10**, 1421 (1974)] and  $5.59 \pm 0.05$  [J. Asikainen and T. Ala-Nissila, *Phys. Rev. E* **61**, 5002 (2000)].
- [17] See supplementary material at <http://link.aps.org/supplemental/10.1103/PhysRevLett.104.215902> for a brief description of the derivation of Eqs. (1), (2), and (4).
- [18] P. Keblinski and F. Cleri, *Phys. Rev. B* **69**, 184201 (2004).
- [19] J.-P. Vassal *et al.*, *Phys. Rev. E* **77**, 011303 (2008).
- [20] A. N. Volkov and L. V. Zhigilei, *J. Phys. Chem. C* **114**, 5513 (2010).
- [21] L. V. Zhigilei, C. Wei, and D. Srivastava, *Phys. Rev. B* **71**, 165417 (2005).